JACS
JOURNAL OF THE AMERICAN CHEMICAL SOCIETY
Article
pubs.acs.org/JACS

Structure Elucidation of Mixed-Linker Zeolitic Imidazolate Frameworks by Solid-State ^{1}H CRAMPS NMR Spectroscopy and Computational Modeling

Krishna C. Jayachandrababu,[†,∥] Ross J. Verploegh,[†,∥] Johannes Leisen,[‡] Ryan C. Nieuwendaal,[§] David S. Sholl,[†] and Sankar Nair*[,†]

[†]School of Chemical & Biomolecular Engineering, Georgia Institute of Technology, Atlanta, Georgia 30332-0100, United States
[‡]School of Chemistry and Biochemistry, Georgia Institute of Technology, Atlanta, Georgia 30332-0400, United States
[§]Materials Science and Engineering Division, National Institute of Standards and Technology, Gaithersburg, Maryland 20899-8550, United States

Supporting Information

ABSTRACT: Mixed-linker zeolitic imidazolate frameworks (ZIFs) are nanoporous materials that exhibit continuous and controllable tunability of properties like effective pore size, hydrophobicity, and organophilicity. The structure of mixed-linker ZIFs has been studied on macroscopic scales using gravimetric and spectroscopic techniques. However, it has so far not been possible to obtain information on unit-cell-level linker distribution, an understanding of which is key to predicting and controlling their adsorption and diffusion properties. We demonstrate the use of ^{1}H combined rotation and multiple pulse spectroscopy (CRAMPS) NMR spin exchange measurements in combination with computational modeling to elucidate potential structures of mixed-linker ZIFs, particularly the ZIF 8-90 series. All of the compositions studied have structures that have linkers mixed at a unit-cell-level as opposed to separated or highly clustered phases within the same crystal. Direct experimental observations of linker mixing were accomplished by measuring the proton spin exchange behavior between functional groups on the linkers. The data were then fitted to a kinetic spin exchange model using proton positions from candidate mixed-linker ZIF structures that were generated computationally using the short-range order (SRO) parameter as a measure of the ordering, clustering, or randomization of the linkers. The present method offers the advantages of sensitivity without requiring isotope enrichment, a straightforward NMR pulse sequence, and an analysis framework that allows one to relate spin diffusion behavior to proposed atomic positions. We find that structures close to equimolar composition of the two linkers show a greater tendency for linker clustering than what would be predicted based on random models. Using computational modeling we have also shown how the window-type distribution in experimentally synthesized mixed-linker ZIF-8-90 materials varies as a function of their composition. The structural information thus obtained can be further used for predicting, screening, or understanding the tunable adsorption and diffusion behavior of mixed-linker ZIFs, for which the knowledge of linker distributions in the framework is expected to be important.

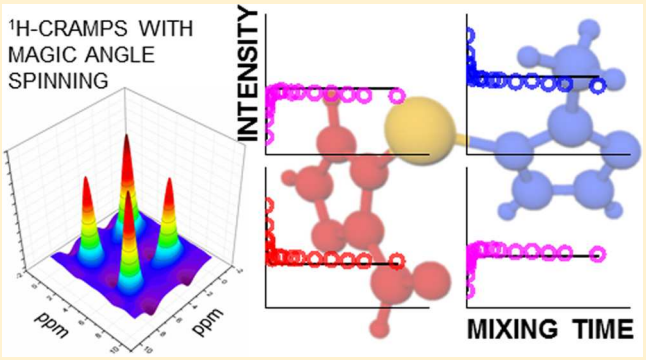

1. INTRODUCTION

Zeolitic imidazolate frameworks (ZIFs) are a subclass of metal−organic frameworks (MOFs)[1−3] that have created great interest for potential use as adsorbents and membrane materials in gas and liquid separation processes.[4−12] ZIFs have metal-atom centers (such as Zn or Co) which are connected by imidazolate linkers to form 3D frameworks. ZIF structures exist in a wide variety of zeolite-like topologies, with a range of cage and window sizes appropriate for molecular separations.[3] In addition to their structural diversity as well as selective adsorption and transport properties for hydrocarbons, other organic molecules, and water, several ZIFs also exhibit good thermal and chemical stability.[13,14] In contrast to ZIFs containing a single type of linker, it has been shown that by incorporating two linkers in the same framework in different relative compositions, one can finely and continuously tune the pore size and host−guest interactions of ZIF frameworks.[15,16] This considerably increases the possibilities for using ZIF structures as a platform for engineering optimal materials for target separation applications without undertaking extensive de novo design and synthesis of ZIFs. For example, Eum et al.[17] and Rashidi et al.[18] recently demonstrated the continuous tuning of hydrocarbon and alcohol diffusivities over several orders of magnitude by varying the relative composition of ZIF-7, ZIF-8, and ZIF-90 linkers in mixed-linker ZIF-8-90 and

Received: March 15, 2016
Published: May 23, 2016

DOI: 10.1021/jacs.6b02754
J. Am. Chem. Soc. 2016, 138, 7325−7336

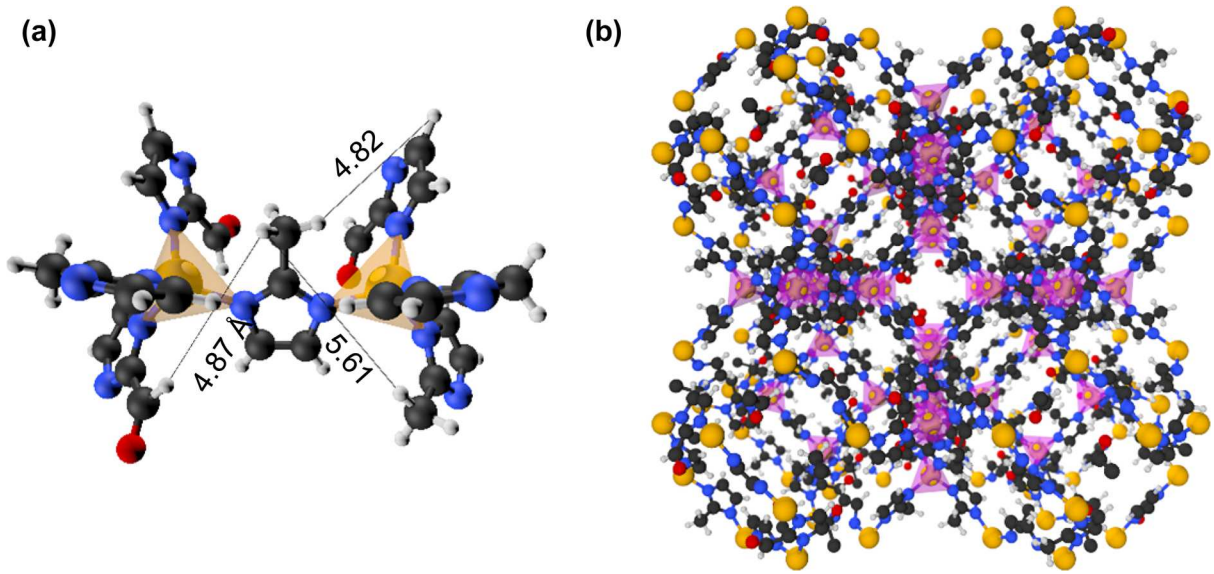

Figure 1. (a) Schematic demonstrating nearest neighbor convention based on bond connectivity where the central mIm linker has 3 OHC-Im and 3 mIm NNs. (b) Schematic of a ZIF-8_{50}-90_{50} hybrid 2 × 2 × 2 supercell where the OHC-Im linkers are randomly distributed. Atom representations are as follows: O = red, *N* = blue, H = off-white, C = black, and Zn = gold. Yellow (a) and purple (b) tetrahedrons are included to illustrate the 4-coordinated Zn atoms.

ZIF-7-90 materials. Based on evidence from water adsorption and micro-Raman measurements, it was also shown that these mixed-linker ZIF materials incorporate both types of linkers in the same crystal and are not physical mixtures of single-linker ZIFs. However, no direct information about the unit-cell-level distribution/mixing of linkers could be gained from these measurements. The distribution of linkers lining the windows determines the pore sizes and shapes, and thereby the diffusion rate of molecules through the pores. In related work, several studies have demonstrated the use of computational techniques to screen ZIFs as potential candidates for specific separation processes.[19−23] However, it is not currently possible to simulate or predict the properties of experimental mixed-linker ZIFs, since the molecular-level linker mixing characteristics of these materials are unknown. Understanding the spatial distribution of the linkers in mixed-linker frameworks is expected to be important in understanding how adsorption and diffusion properties can be controlled, and furthermore in selecting or designing appropriate linker combinations and compositions for a targeted separation process.

Due to the large degree of compositional disorder in mixed-linker ZIFs, crystallographic techniques cannot be used as a primary method for elucidating their structure. However, solid-state NMR spectroscopy can distinguish between the nuclear environments of different functional groups, for example in the study of domain sizes in block copolymers.[24−27] Recently several groups have demonstrated the use of NMR spectroscopy to study structural properties of MOFs. Rossini et al. used DNP-enhanced NMR spectroscopy to obtain rapid, high S/N ratio measurements of the presence and qualitative location (e.g., surface versus bulk) of functional groups in several compositional variants of the MOF (In)-MIL-68.[28] Baias et al. used ^{1}H NMR spectroscopy in conjunction with X-ray crystallography to determine the local structure of a substituted imidazole based MOF (SIM-1).[29] With this technique, it was possible to deduce the relative orientation of functional groups that were present on the same linker molecule and their distribution within the framework. It was shown by Kong et al. that rotational echo double resonance (REDOR) NMR can be used to estimate the linker distribution in multivariate (MTV) MOFs.[30] This technique requires isotopic labeling with ^{13}C and ^{15}N nuclei, since ^{13}C is only 1.1% naturally abundant (and hence insensitive), and ^{14}N is a spin-1 nucleus (which is less amenable to REDOR). Kranjc et al. reported ^{1}H NMR spin diffusion experiments which showed that the large difference in the (known) ordered distributions of linkers in two aluminum-based MOFs (DUT-5) could be distinguished when using 20 kHz magic angle spinning (MAS) and RFDR ^{1}H−^{1}H recoupling.[31] Here, we demonstrate the use of ^{1}H combined rotation and multiple pulse spectroscopy (CRAMPS) spin diffusion experiments with 5 kHz MAS and no recoupling in conjunction with computational modeling of mixed-linker ZIFs for estimating the linker distributions in multiple mixed-linker ZIF materials that are all mixed on size scales of ≈1 nm, which is a significant departure from previous work. We focus particularly on ZIF-8-90 hybrids as a typical example for such a challenging system and note that routine Fickian-based spin diffusion analysis protocols cannot be used for distinguishing structures on these short length scales. The linker distributions in these materials are unknown a priori. This methodology does not require isotopic enrichment for the NMR measurements, and allows a more generalized way of determining the structures of mixed-linker MOFs when one assumes a relatively simple, phenomenological spin exchange model. When two different types of linkers (with NMR-distinguishable protons) are distributed ("mixed") in the framework, the distribution of nearest neighbor internuclear distances between the two functional groups will depend upon the degree of mixing. For example, in a clustered linker distribution (where each type of linker forms isolated phases) the distance distribution between linkers of two different types will be very different from more random or highly ordered linker distributions. By measuring spin exchange rates using NMR, and matching them to dipolar couplings calculated from the proton positions from

DOI: 10.1021/jacs.6b02754
J. Am. Chem. Soc. 2016, 138, 7325−7336

computationally generated models, one can ascertain the level of linker mixing in the materials of interest.

We have used the short-range order (SRO) as defined by the Warren-Cowley parameter α to quantify the degree of linker mixing.[32] This parameter is defined as

$$\alpha_j = 1 - \frac{P_j^{A(B)}}{x_B} \quad (1)$$

where $P_j^{A(B)}$ is the conditional probability of finding the linker of type B at the j^{th} neighbor site given a linker of type A, and x_B is the fractional composition of linker type B in the material. For hybrid ZIF-8-90 systems, we have selected the nearest neighbor ($j = 1$) to define α. Nearest neighbors (NNs) are not assigned based on the value of the distance but are based upon the sharing of a common Zn^{2+} center; therefore, each organic linker has 6 NNs. The contribution of second order NNs, (i.e., those connected through two Zn metal centers) are assumed to be negligible (see below). Figure 1a shows the NN convention, and Figure 1b shows a schematic of a ZIF-8_{50}-90_{50} hybrid 2 × 2 × 2 unit cell in which the linkers are randomly distributed. The experimentally measured spin diffusion curves of different mixed-linker ZIFs can be compared to the computationally generated spin diffusion curves of structures with different SROs to identify the value of α that best describes the synthesized material. Note that for the calculation of spin exchange rates, multiple quantum effects, magic angle spinning effects, molecular dynamics, and long-range couplings are ignored. The physical significance of this short-range order is demonstrated by showing how the window-type distribution varies as a function of α. Since the diffusion of guest molecules through the cages of a ZIF material is governed by the type of linkers that line the window, this distribution is critical in determining how material transport is a function of the relative composition of constituent linkers.

2. EXPERIMENTAL METHODS

Pure ZIF-8 and ZIF-90 were synthesized according to a previously reported procedure.[33] The ZIF-8_x-90_{100-x} ($0 < x < 100$) hybrid materials were made by the procedures given in Thompson et al.[15] Zinc nitrate hexahydrate and 2-methylimidazole (mIm, ZIF-8 linker) were obtained from Sigma-Aldrich; imidazole-2-carboxaldehyde (OHC-Im, ZIF-90 linker) and sodium formate from Alfa Aesar; methanol and *N*,*N*-dimethylformamide were obtained from BDH Chemicals. All chemicals were used in the syntheses without further modifications or purification. Details of the synthesis of ZIF-8-90 materials, and characterization procedures for all the materials, are given in the Supporting Information. NMR measurements were performed on a Bruker Avance III 400 MHz spectrometer using a standard broadband H/X MAS probe. The samples (~5 mg) were loaded into 4 mm ZrO_2 rotors, and the magic angle spinning was intentionally set to a relatively low rate (5 kHz) so as to avoid the quenching of spin diffusion; experiments performed at faster rates exhibited long onset times. No recoupling was applied during the mixing time. 2D CRAMPS experiments were conducted using the phase modulated Lee−Goldburg decoupling during the evolution and detection times (Bruker Pulse sequence: wpmlg2d).[34−36] While slightly different resolutions may be achieved using an alternative homonuclear decoupling CRAMPS technique (e.g., BR-24 or DUMBO), the results would not be affected since no pulses occur during the mixing time. The possibility of spatially heterogeneous spin temperatures, or spatial polarization gradients, should not affect the results of these 2D experiments, but could affect a 1D variation of this experiment.[37] Mixing times ranging from 0.05 to 50 ms were used to study the temporal evolution of spin diffusion. Other typical experimental parameters were 399.92 MHz Larmor frequency, 2.5 μs $\pi/2$ pulse width, 56.57 kHz frequency offset, 12.5 μs Lee−Goldburg 2π pulse, receiver gain of 8, 4 scans, and 512 × 128 2D points with sine apodization.

3. SIMULATION METHODS

3.1. ZIF-8_x-90_{100-x} Structure Generation. The starting ZIF-8 unit cell (structure code VELVOY[1]), and the ZIF-90 unit cell (structure code WOJGEI[38]) were taken from the Cambridge structural database (CSD).[39] As a standard self-consistency check, the geometries of these two bulk ZIF structures were energy minimized using plane wave density functional theory (DFT) calculations as implemented in the Vienna Ab initio package (VASP)[40,41] version 5.2.12. The generalized gradient approximation (GGA) Perdew−Burke−Ernzerhof (PBE)[42] functional was applied along with D2 dispersion corrections by Grimme.[43] Calculations were performed at the Γ-point with a 700 eV energy cutoff. Atomic forces were converged to <0.03 eV/Å during both unit cell and atomic position relaxations. The unit cells for the two ZIFs were subsequently expanded into 5 × 5 × 5 supercells. The 5 × 5 × 5 supercells were not reoptimized after linker swapping since they comprised anywhere between 31 500 and 34 500 atoms depending on the composition. DFT structure optimizations would be computationally infeasible on a supercell of such large sizes. Small displacements (~0.1 Å) in the atomic positions of the hydrogens are not expected to have a large effect on the spin diffusion predictions. Interatomic distances between the $-CH_3$ and $-OHC$ hydrogens on the order of >10 Å would have a greater impact on the spin diffusion behavior.

A linker NN library was generated through the mIm connectivity determined using a fast percolation algorithm.[44] Using this library of linker NNs a simple reverse Monte Carlo (RMC) procedure was implemented to generate a new linker NN library with a characteristic SRO and specified composition. A candidate linker swap that generated a NN library with a SRO closer to the target SRO, α_t, was accepted with unit probability and unfavorable moves were accepted with probability $\exp(-\beta|\alpha - \alpha_t|)$ following from the Metropolis criterion. Values of β ranged from 1 to 1000 for different target SRO values and a total of 1×10^6 MC steps were used. A fraction of mIm linkers were then chosen to be swapped with OHC-Im linkers using the final linker NN library. This procedure was implemented by aligning the imidazole ring plane normal vectors as well as the vectors defined by the primary carbon and the nitrogen−nitrogen centers-of-mass of an OHC-Im fragment and chosen mIm linker. Organic linker fragments were taken from the DFT energy optimized bulk structures. Several representative hybrid ZIF-8_x-90_{100-x} XRD patterns calculated using Mercury CSD 3.5.1[45−48] are available in the Supporting Information.

3.2. Semi-Empirical Fitting of ^{1}H CRAMPS NMR Intensity Curves. Simulated NMR intensity fit curves were generated using a kinetic model of spin exchange/diffusion using modeled proton positions as described by Perrin and Dwyer as well as Elena and Emsley.[30,49−51] This analysis assumes that relaxation of the z-(longitudinal) magnetization (parallel to the applied static magnetic field) back to its equilibrium value during spin diffusion experiments can be modeled through a system of coupled differential equations. All details of the model along with relevant equations and parameters are given in the Supporting Information. This set

DOI: 10.1021/jacs.6b02754
J. Am. Chem. Soc. 2016, 138, 7325−7336

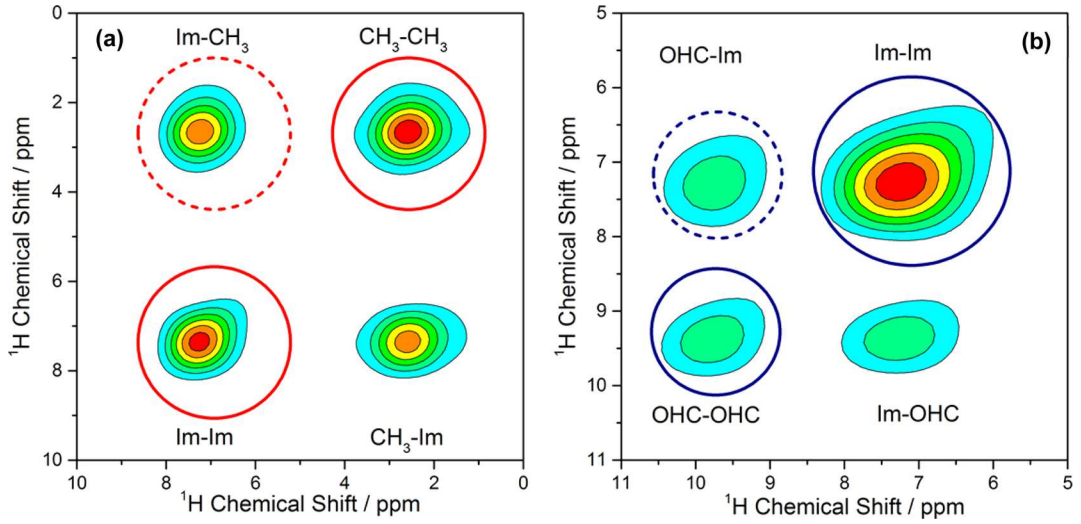

Figure 2. ^{1}H NMR contour plots of (a) ZIF-8 and (b) ZIF-90, measured at 5 kHz MAS and 1 ms mixing time. Diagonal peaks are marked in solid circles and cross-peaks in dashed circles.

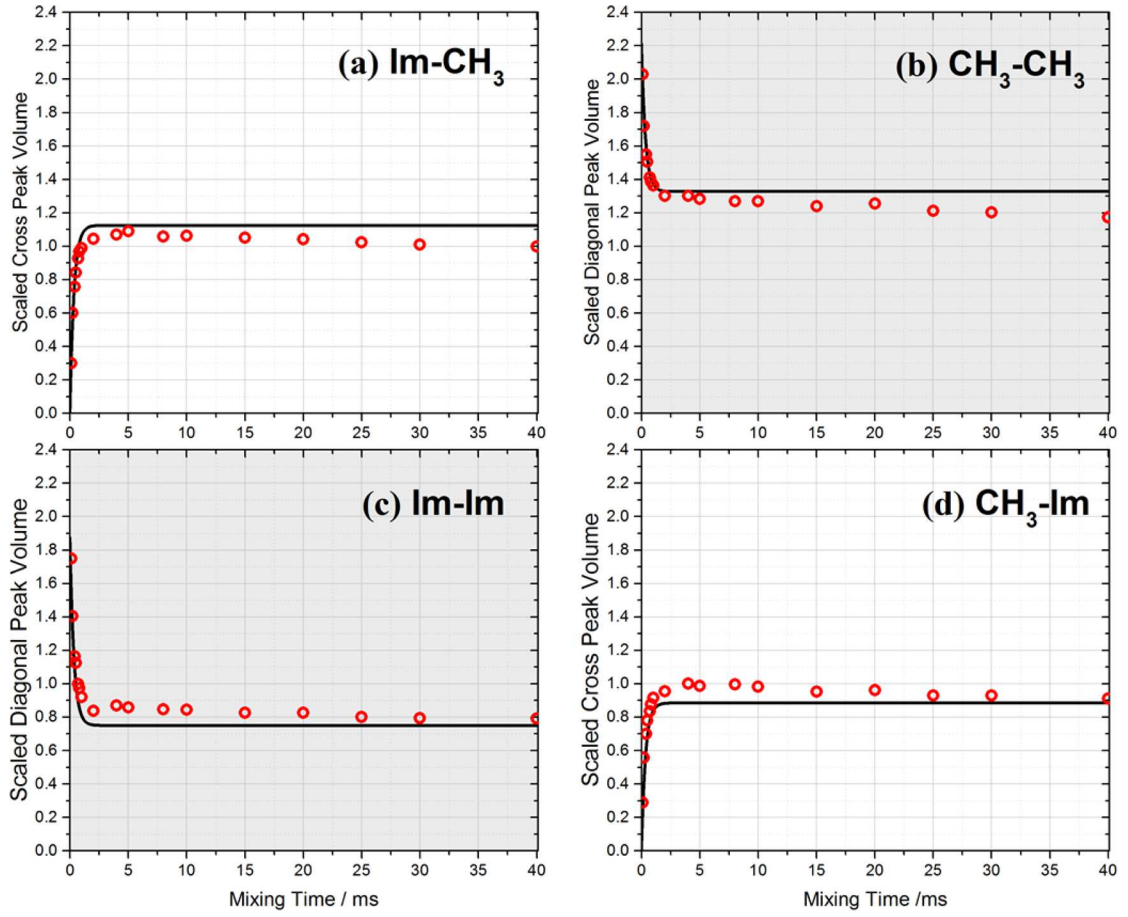

Figure 3. Fit of the spin-exchange model (solid curves) to experimental CRAMPS NMR measurements (red circles) for spin exchange between protons in ZIF-8 as a function of the mixing time.

of kinetic equations models the spin exchange behavior using the r^{-6} dependence of the exchange rate due to the dipolar coupling and assumes spin−lattice relaxation occurs on time scales greater than even the longest mixing time.[52−54] To assess agreement between simulated and experimental ^{1}H NMR spectrual intensities at various values of r, we utilized the mean absolute error (MAE):

$$\mathrm{MAE} = \frac{1}{n}\sum_{k=1}^{n} |I_{\mathrm{sim}} - I_{\mathrm{exp}}| \quad (2)$$

where n is the number of data points and the subscripts "sim" and "exp" refer to simulated and experimental values, respectively. We generated mixed-linker ZIF structures spanning the range of SRO values for a fixed composition.

DOI: 10.1021/jacs.6b02754
J. Am. Chem. Soc. 2016, 138, 7325−7336

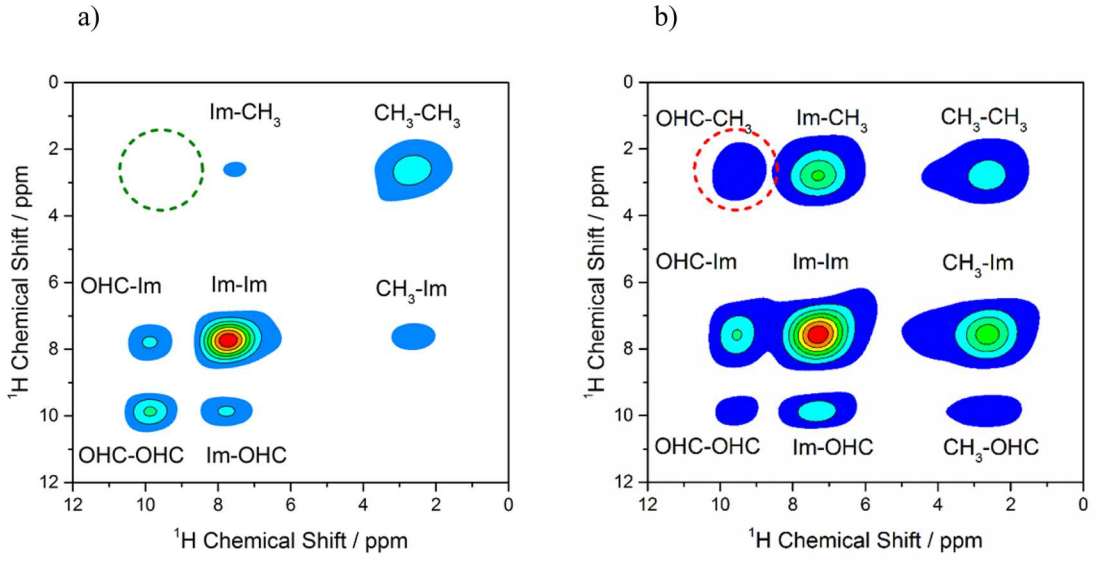

Figure 4. ^{1}H NMR spectra of (a) physical mixture of ZIF-8 and ZIF-90 and (b) mixed-linker ZIF-8_{50}-90_{50}, measured at 5 kHz MAS and 50 ms mixing time. Green dotted circle in (a) denotes the absence of transfer between methyl and aldehyde protons in physical ZIF mixture. Red dotted circle in (b) shows the transfer in hybrid material.

From this set, we determined the structure with the minimum MAE and reported a confidence interval on the corresponding SRO. The SRO confidence interval is defined from the SROs that correspond to structures that yield MAE values within ±5% of the minimum MAE structure.

4. RESULTS AND DISCUSSION

4.1. Pure ZIF-8 and ZIF-90 NMR Analysis. The ^{1}H chemical shift signatures of the methyl group (2.6 ppm), aldehyde group (9.8 ppm), and the protons on the 4- and 5-positions of the imidazole rings (7.3 ppm) in ZIF-8 and ZIF-90 were first identified using solution NMR of samples digested in d_4-acetic acid. Based upon initial survey measurements, the spinning frequency for spin diffusion data collection was fixed at an optimum of 5 kHz. The selection of spinning frequency is important since there is a trade-off between the spectral resolution and strong dipolar coupling. At lower frequencies, the solid-state spectra were not sufficiently resolved, whereas at higher frequencies the averaging of dipolar couplings slowed down spin diffusion and yielded a significant deviation from $t^{1/2}$ behavior. Figures 2a–b show ^{1}H NMR spectra for ZIF-8 and ZIF-90 and example contour plots of the two materials from the CRAMPS experiment at 1 ms mixing time. The diagonal peaks (marked by solid circles) are a result of direct observation of methyl and imidazole protons. The cross peak (marked by dashed circle) is caused by magnetization transfer between the nuclei corresponding to the diagonal peaks. The presence of this cross peak shows that there is intimate contact between the imidazole protons and the methyl protons in ZIF-8 as well as the imidazole protons and aldehyde proton in ZIF-90.

The CRAMPS NMR data from the two pure ZIFs were fitted to the kinetic spin exchange model (Equations S2–S8, Supporting Information) to determine the single parameter A in the spin exchange rate-constant matrix (Equation S6, Supporting Information). Scaled experimental diagonal and cross-peak volumes as a function of mixing time, along with the model fits, are reported for ZIF-8 in Figure 3, and the results for ZIF-90 are shown in the Supporting Information. The obtained values for ZIF-8 and ZIF-90 are 101.8 ± 5.7 and 120.7 ± 8.1, respectively. The values of initial z-magnetization (Equation S5, Supporting Information) for the −Im and $-CH_3$ diagonal peaks were set as the average values from the sum of the diagonal and cross peak volumes (e.g., CH_3−Im + CH_3−CH_3 and Im−Im + Im−CH_3) at mixing times between 2 to 40 ms. While the A values for the hybrid (mixed-linker) ZIFs are expected to all be similar based on the end-member ZIFs, for completeness we calculated A parameters for each of the mixed-linker ZIFs using a weighted geometric mean based upon the fractions of each type of linker in the mixed-linker material. The three initial z-magnetization values for the hybrid materials were set using the same methodology as described above. Only the interatomic distances between the $-CH_3$, −Im, and −OHC hydrogens were changed in the various atomic models based on their different short-range order values.

4.2. ZIF-8_x-90_{100-x} Hybrid Materials. Figure 4a shows the CRAMPS contour plot at 50 ms mixing time from a sample consisting of equal amounts of pure ZIF-8 and pure ZIF-90 crystals mixed physically. As expected, cross-peaks for the methyl-to-imidazole-ring and aldehyde-to-imidazole-ring spin transfers are observed to arise from within the individual ZIF-8 and ZIF-90 phases since spin transfer occurs over length scales ranging from a few angstroms to tens of nanometers (within the time window of the experiment). However, no methyl-to-aldehyde exchange is observed (dashed green circle) which is consistent with the crystal sizes of the ZIF samples being above 100 nm. In contrast, the 2D CRAMPS contour profile for a ZIF-8_{50}-90_{50} sample collected at 1 ms mixing time is shown in Figure 4b. Spin transfer between methyl protons and aldehyde protons is clearly observed from the cross-peak at the expected position (dashed red circle).

Intensity profiles at several mixing times were used to study the spin diffusion and quantify the length scale of these transfer processes. ZIF-8 and ZIF-90 were used for calibration since the distances between the functional group and imidazole ring protons on each linker are known from their crystal structures.[54] Spin diffusion is the spontaneous exchange of spin

DOI: 10.1021/jacs.6b02754
J. Am. Chem. Soc. 2016, 138, 7325–7336

polarization between nuclear spins, and the rate of this exchange is a function of the domain sizes that comprise the participating nuclei.[52] The intensity, which is defined as the ratio of the cross-peak area to the cross-peak and source-peak sum, is plotted versus the square root of the mixing time and shown in Figure 5a for both ZIF-8 and ZIF-90. Each spin diffusion profile shows an approximately linear increase from 0−2 $ms^{1/2}$ followed by a plateau at longer mixing times. The saturation levels of these curves are defined by the relative ratio of protons in the source and the sink, which in this case are the methyl and aldehyde protons, respectively.[24]

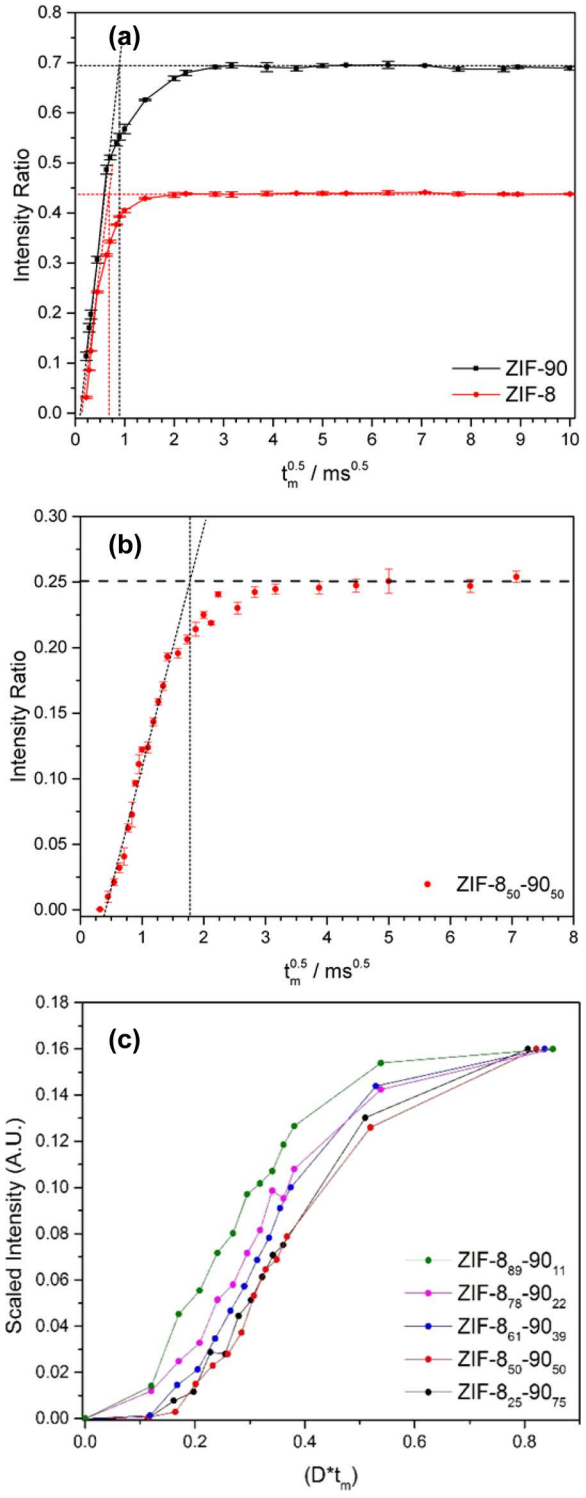

Figure 5. Spin diffusion profiles of (a) ZIF-8 and ZIF-90, (b) ZIF-8_{50}-90_{50}, and (c) ZIF-8-90 at various compositions scaled by the anticipated spin diffusion coefficient.

For an estimation of the spatial distribution of linkers, one can adopt a Fickian-based spin diffusion approach. A useful feature of this approach is that the domain size(s) of hybrids can be determined simply by the extrapolation of the early time, linear portion of the slope to the *x*-asymptote when plotted as a function of the square root of time.[55] In this case, the two unknowns are the dimensionality of the domains (spheres, rods, fractals, lamella, etc.) and the spin diffusion coefficient. An alternative technique such as transmission electron microscopy or small-angle X-ray diffraction is required to determine the dimensionality of the domains. The spin diffusion coefficient can be estimated via empirical relations or using standards of known length scales of mixing.[24] We estimated the spin diffusion coefficients in the ZIF-8 and ZIF-90 neat materials by inspecting the proton positions in the crystal structures and performing finite element calculations of the spatial polarization changes using a lamellar model of packing of protons (Figure S7, Supporting Information) for various spin diffusion coefficient values. The best fit values were 0.25 nm^2/ms and 0.2 nm^2/ms for ZIF-8 and ZIF-90, respectively, which is on the lower end of reported ^{1}H spin diffusion coefficients (0.05−0.8 nm^2/ms) and is likely due to proton diluteness compared to typical polymers.[26,56]

An alternative way for determining the spin diffusion coefficient *D* was introduced by White et al.[26] as represented by the following equation:

$$D = \frac{\pi x^2}{4\epsilon\tau_{eq}} \tag{3}$$

where x is the distance of the defined irreducible unit or domain as measured from the crystal structure, ϵ is the dimensionality of spin transfer, and τ_{eq} is the observed magnetization equilibration time. For intramolecular spin diffusion the characteristic dimension $\langle x \rangle$ of the domain was estimated using

$$\langle x \rangle = (Ld)^{0.5} \tag{4}$$

where L is the length and d is the diameter of the domain. For ZIF-8 and ZIF-90, x was estimated at 0.35 and 0.34 nm respectively from the crystallographic structures (Figure S8, Supporting Information). τ_{eq} was evaluated by extrapolating the linear region of the spin diffusion curve to the saturation level as shown in Figure 5a, and was found to be 0.43 ms for ZIF-8 and 0.74 ms for ZIF-90. The values of $D_{ZIF\text{-}8}$ and $D_{ZIF\text{-}90}$ obtained using these parameters and eq 3 are 0.2 nm^2/ms and 0.1 nm^2/ms, respectively.

Figure 5b shows the spin diffusion plot for a ZIF-8_{50}-90_{50} mixed-linker material. The expected saturation level (at long mixing times) of the spin diffusion curve for this composition is also shown. This can be calculated purely from the bulk composition by taking the ratio of numbers of source and sink protons. For example, in ZIF-8_{50}-90_{50} there are 3 methyl protons for every aldehyde proton and hence the expected saturation ratio was calculated as $1/(1 + 3) = 0.25$. τ_{eq} was estimated at 3.1 ms by extrapolating the slope to the asymptote. The corresponding value of x calculated using Equation 3 is ≈1 nm; note that the dimensionality (ϵ) is not known a priori. We also compared the spin diffusion data for

DOI: 10.1021/jacs.6b02754
J. Am. Chem. Soc. 2016, 138, 7325−7336

the multiple compositions of ZIF-8_x-90_{100-x}. Since the spin diffusivity is likely to change (subtly) among the samples because of changes in the proton density and (potentially) molecular dynamics, we scaled the spin diffusion data for the multiple compositions by the anticipated spin diffusion coefficient. The spin diffusion coefficients were calculated by either interpolating between the ZIF-8 and ZIF-90 using either a geometric average or by using the second moment of the single pulse excitation spectra (Figures S9 and S10, Supporting Information) for use in known equations of the spin diffusion coefficient. Both methods yielded similar results. The data are shown in Figure 5c, where we have scaled the asymptotes to coincide and have zoomed into the early time points. As shown in the figure, all of the compositions have nearly the same total equilibration time, $(Dt)^{0.5} \approx 0.9$, which suggests that the total repeat units of the domains in ZIF-8_x-90_{100-x} materials are nearly identical at a length scale comparable to their XRD-derived cavity diameters as measured with Zeo++[57] for ZIF-8 (1.14 nm)[1] and ZIF-90 (1.136 nm),[38] and also to the size of their unit cells (1.699 and 1.727 nm respectively). Previously, there had been no direct evidence of linker mixing in ZIFs at subunit-cell length scales. While previous findings that employed techniques including micro-Raman spectroscopy, photothermal induced resonance (PTIR), and aerosol time-of-flight mass spectrometry (ATOF-MS) for observing spatial uniformity in mixed-linker MOFs have been limited to length scales greater than 100 nm,[18] the above NMR spin diffusion measurements conclusively establish that there is subunit-cell linker mixing in these mixed-linker ZIFs. However, in order to delineate further between these structures, we turned to a kinetic exchange model.

The spin equilibration times (scaled by the estimated spin diffusion coefficients) are approximately the same among the compositions, which denotes the same total repeat distance in each of the samples. The 50:50 composition exhibits the slowest initial slope, denotes the largest possible domain, and decreases in composition of either of the components only serve to decrease the average cluster size and increase the slope, an observation consistent with previously determined Fickian models. However, we also observe a drastic deviation from the classic Fickian $t^{1/2}$ dependence upon decreasing the ZIF-8 fraction. Chen et al.[58] have shown that local (<1 nm) spin diffusion coefficients can be slower than those at longer length scales due to nondiffusive, exponential behavior due to discrete exchange events. Here, it seems the time window over which this occurs varies with sample and is likely due to the composition-dependent change in the uniformity of local dipolar fields under MAS. Upon inspection of the single pulse excitation ^{1}H MAS NMR spectra (Supporting Information), the ZIF-8-rich materials exhibit only weak MAS sideband intensity, which would suggest a strong network of dipolar coupled protons, little appreciable dipolar field averaging, and more uniform dipolar fields. The ZIF-90-rich hybrids, on the other hand, exhibit NMR spectra with strong sideband intensities with no appreciable underlying broadened features, suggesting significant averaging of weak couplings in the presence of strong couplings and less uniform dipolar fields.

Next we explore the possibility of determining more quantitatively the short-range linker mixing patterns. Several groups have used ^{1}H spin diffusion NMR as a method for predicting proton positions using rates of exchange between neighboring protons using kinetic equations. We created models of mixed-linker ZIFs that had the same relative linker compositions but different SRO (α) values, via methods described in a previous section. The Warren Cowley parameter, used to quantify SRO, is normalized to cover the range from $[-1, 1]$. A system with an α value of 1 (-1) is completely clustered (ordered). For the periodic systems under consideration, the SRO of clustered structures can asymptotically approach 1 with increasing unit cell size since there will always be an interface between regions containing only linkers of one type. The lower bound (~ -0.29), as determined through our RMC procedure, is observed to be constant for a composition range of 0.21 to 0.79 mole fraction of OHC-Im linkers. This observable lower limit is due to our definition of nearest neighbors as well as the specific topology of our ZIF system. The lower limit on the SRO parameter may not be possible to determine a priori for all 3D periodic systems and would need to be determined empirically for specific systems as in the present case. Figure 6 shows how the functional group protons ($-C\mathbf{H}_3$ for ZIF-8 and $-C\mathbf{H}O$ for ZIF-90) are distributed in space over a 5 × 5 × 5 unit-cell volume for ZIF-8_{50}-90_{50} with three different values of α

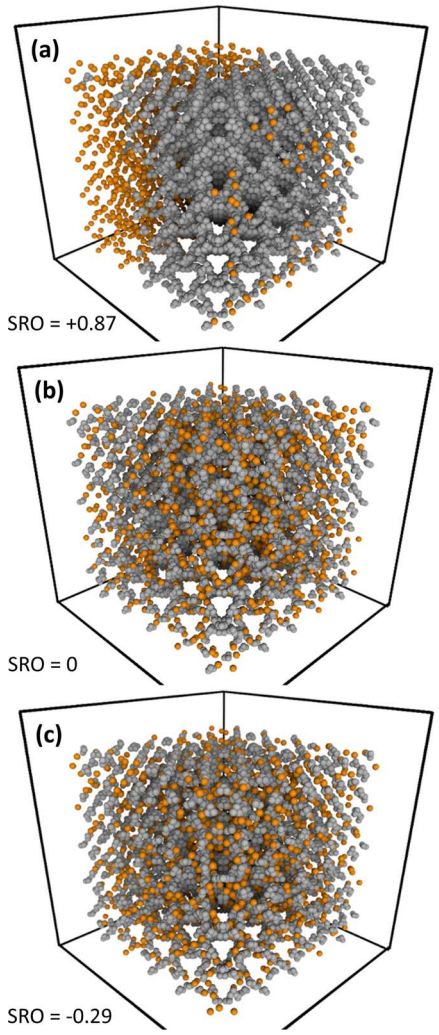

Figure 6. ZIF-8_{50}-90_{50} methyl (gray) and aldehyde (orange) hydrogen maps for 5 × 5 × 5 supercells of size 8.47 nm: (a) SRO of α = 0.87 demonstrating extreme clustering, (b) SRO of α = 0.0 demonstrating a random linker arrangement, and (c) SRO of α = −0.29 demonstrating partial ordering. Hydrogens not to scale, in order to enhance clarity.

DOI: 10.1021/jacs.6b02754
J. Am. Chem. Soc. 2016, 138, 7325−7336

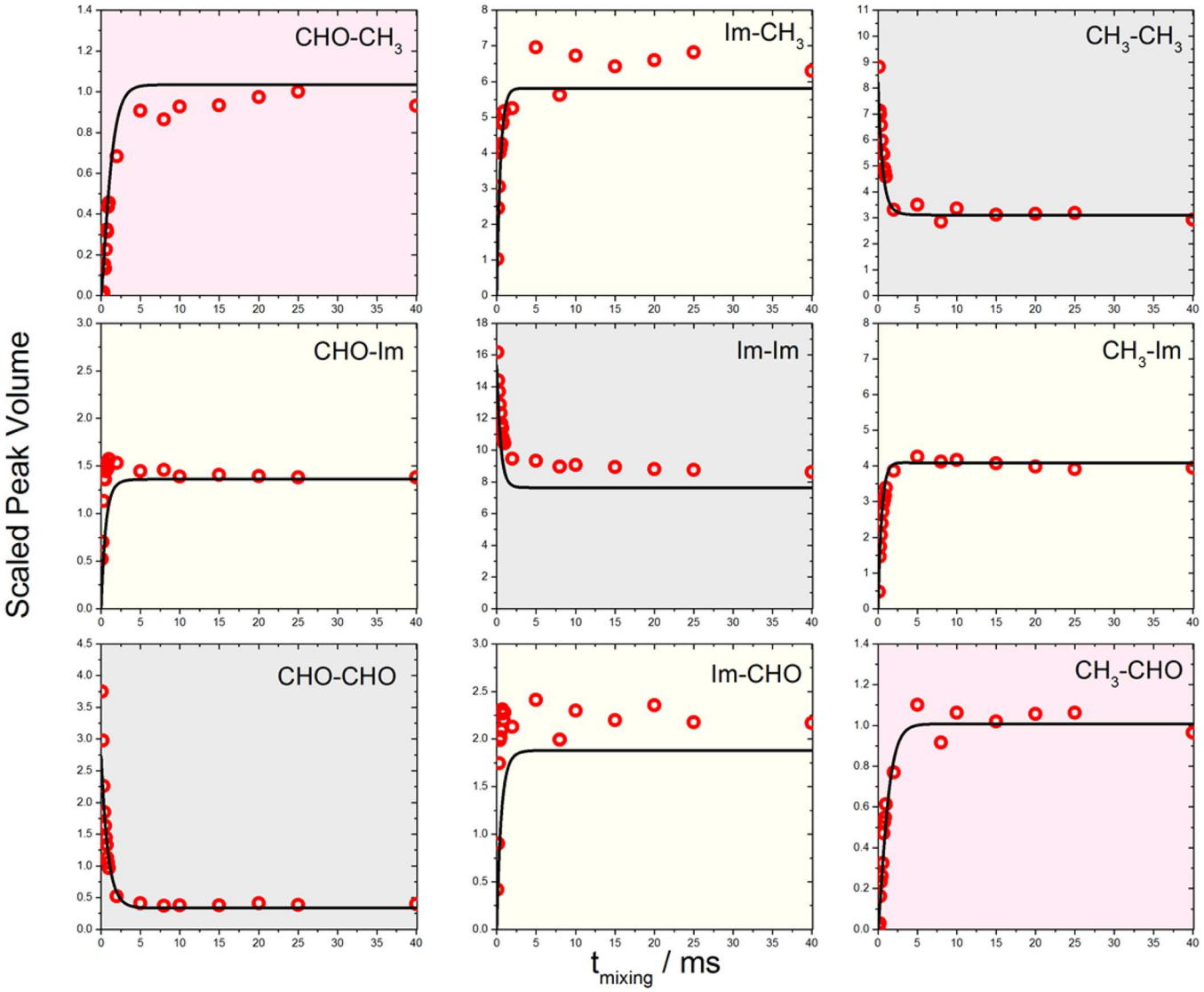

Figure 7. Experimental (open red circles) and simulated NMR spin exchange peak intensities for ZIF-8_{50}-90_{50} with α = 0.45.

representing clustering, randomization, and significant ordering, respectively. While Fickian models of spin diffusion could eliminate such a highly clustered model as shown in Figure 6a (SRO = 0.87) as a possibility for the structures here, kinetic models may offer a more precise estimate of varying degrees of randomization and clustering (Figure 6b–c). For each overall composition, simulated ^{1}H CRAMPS NMR intensity patterns for the mixed-linker structures with different α values were directly calculated using nearest-neighbor dipolar couplings (see the Supporting Information). No fitting parameters are used, since the spin exchange parameter A is already known from the calibrations with ZIF-8 and ZIF-90. For example, Figure 7 shows the experimentally measured and calculated peak intensities of ZIF-8_{50}-90_{50} for α = 0.45. The subplots shaded in pink represent NMR spin exchange between methyl protons on the ZIF-8 linker and the aldehyde protons on the ZIF-90 linker, the transfer processes that are of most interest for structure determination; although all the exchange processes are measured and calculated. The agreement between experimental and simulated NMR curves was quantified using MAE (eq 2), which was used to determine the structure that most closely reproduces the experimental data for each mixed-linker ZIF composition. Specifically, we used the intensity ratio of the cross peak corresponding to the methyl-to-aldehyde (CH_3–CHO) transfer to the sum of the intensities of the methyl diagonal peak (CH_3) and the CH_3–CHO peak (as plotted earlier in Figure 5) for assignment of an SRO value. Simulated curves were generated for several structures with identical composition but different short-range-order values.

The comparisons for ZIF-8_{50}-90_{50} are shown in Figure 8. The best minimum MAE between experimental and simulated curves for this material is given by the structure with α = 0.45 (Figure S13, Supporting Information). From the definition of α, it follows that the two linkers in ZIF-8_{50}-90_{50} exhibit some tendency for clustering. The value of α = 0.45 indicates that given a methyl linker in ZIF-8_{50}-90_{50}, there is a 28% probability that there is an aldehyde linker present in each of its six nearest neighbor sites. A ± 5% deviation was chosen as the tolerance limit for describing the structure with reasonable accuracy. It was found that structures with $0.40 < \alpha < 0.55$ fell in this range.

Figure 9 shows the best fits of the spin exchange plots for the various compositions of mixed-linker ZIF-8_x-90_{100-x}

DOI: 10.1021/jacs.6b02754
J. Am. Chem. Soc. 2016, 138, 7325–7336

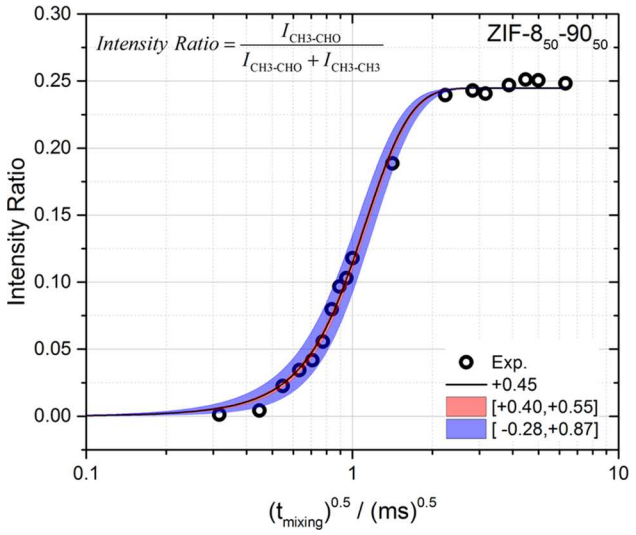

Figure 8. Comparison of experimental NMR spin exchange intensity ratios and simulated curves for several structures with different α values for ZIF-8$_{50}$-90$_{50}$.

materials, and Figure S13 (Supporting Information) shows the MAE versus α for each composition. The model yields good fits for ZIF-8$_{25}$-90$_{75}$, ZIF-8$_{61}$-90$_{39}$, and ZIF-8$_{78}$-90$_{22}$ yield good fits, but ZIF-8$_{89}$-90$_{11}$ shows greater deviation. Recall that ZIF-8$_{89}$-90$_{11}$ yielded a spin diffusion curve with a strong $t^{1/2}$ dependence (Figure 5c) and weak spinning sideband intensity at 5 kHz MAS (Supporting Information), suggesting the strongest network of dipolar couplings of the ZIF-8$_x$-90$_{100-x}$ compositions. Since the kinetic exchange model is based solely on direct couplings and ignores multiple quantum, molecular dynamics, and MAS effects, we therefore posit that the model is most accurate when studying sample sets with less appreciable variation in the local proton density and/or dynamics.

For the compositions that the model is most successful, it was observed that the best-fit α value falls in the range that indicated a close to randomly distributed structure, with the exception of ZIF-8$_{50}$-90$_{50}$. This is represented graphically in Figure 10 in relation to the "nearest neighbor" concept. The anomalous behavior of ZIF-8$_{50}$-90$_{50}$ is not clearly understood at this point. It must be noted that this material certainly shows linker mixing at a unit-cell level and has long-range compositional homogeneity. The variation in α is directly translated to a slightly higher tendency for pore windows to have exclusively ZIF-8 or ZIF-90 linkers (see below). Even though individual windows have different compositions, there are multiple windows of each type within each unit cell and at length-scales higher than that of each unit cell, the composi-

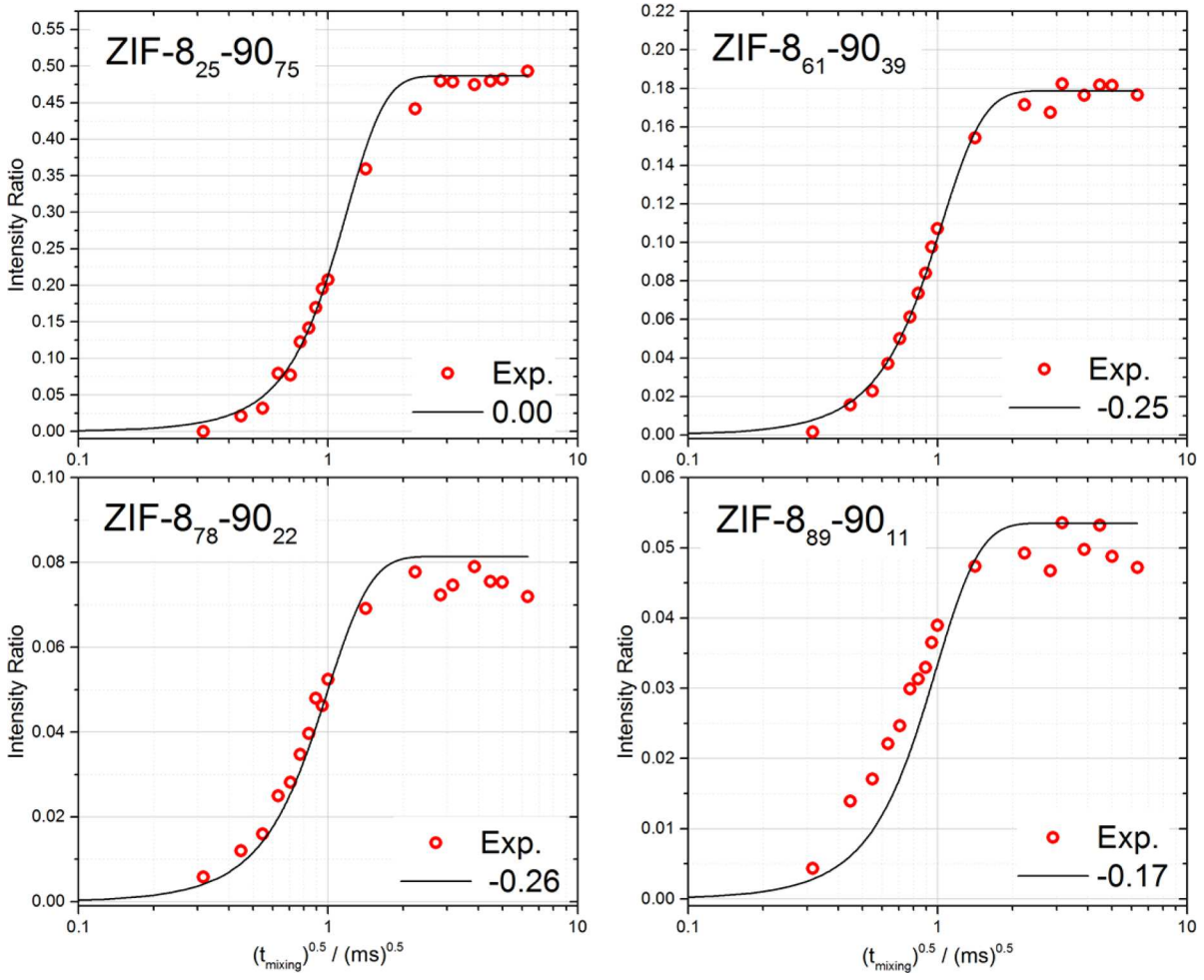

Figure 9. Comparison of experimental (red circles) and simulated 2D CRAMPS peak ratios of the "best-fit" SRO models (solid black lines), for four different ZIF-8–90 mixed-linker materials.

DOI: 10.1021/jacs.6b02754
J. Am. Chem. Soc. 2016, 138, 7325–7336

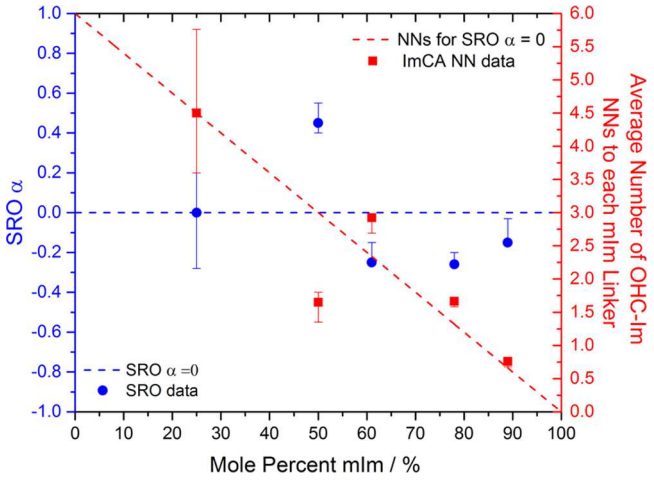

Figure 10. Short range order α and average number of OHC-Im linkers per mIm linker as a function of the overall composition of the mixed-linker ZIF-8-90 material.

tional homogeneity is preserved. We can offer the hypothesis that when both linkers are present in roughly equal amounts, there may be an increased thermodynamic or kinetic driving force that tends toward cluster formation during synthesis. On the other hand, when one linker is in the minority, it may prefer to be more randomly distributed within the "matrix" of the majority linker. Experimentally, it has been observed that the rate of formation of ZIF-8_x-90_{100-x} goes from slow (observable product formation in a duration of many minutes) to fast (nearly instantaneous) as the relative content of the OHC-Im linker is increased from 0 to 100%. The observed deviation from near-random mixing of ZIF-8_{50}-90_{50} could be attributed to competing effects of heats-of-mixing and the reaction kinetics. Although uncommon, such deviations from the expected value of order parameter for binary materials are known. For example, an almost-equiatomic Pd−Pt alloy was shown (via X-ray scattering measurements) to exhibit a more ordered behavior than what was expected based on phase transition thermodynamics.[59]

It has been clearly shown that hybrid cage-type ZIF-8−90 materials allow for drastic tunability of molecular diffusion,[17] implying that diffusion is primarily influenced by the three imidazolate linkers lining the pore windows between cages. These windows can be classified into 4 types: Type 1 (lined by 3 mIm linkers), Type 2 (2 mIm linkers and 1 OHC-Im linker), Type 3 (1 mIm linker and 2 OHC-Im linkers), and Type 4 (3 OHC-Im linkers). The various structure models generated with different compositions and short-range orders can then be differentiated according to the probability distribution of these windows in the structure. A set of 166 unique 5 × 5 × 5 supercells were generated to represent the entire composition and accessible SRO parameter ranges to provide a qualitative understanding of the effect of SRO on window type probability. The probability of window types was determined

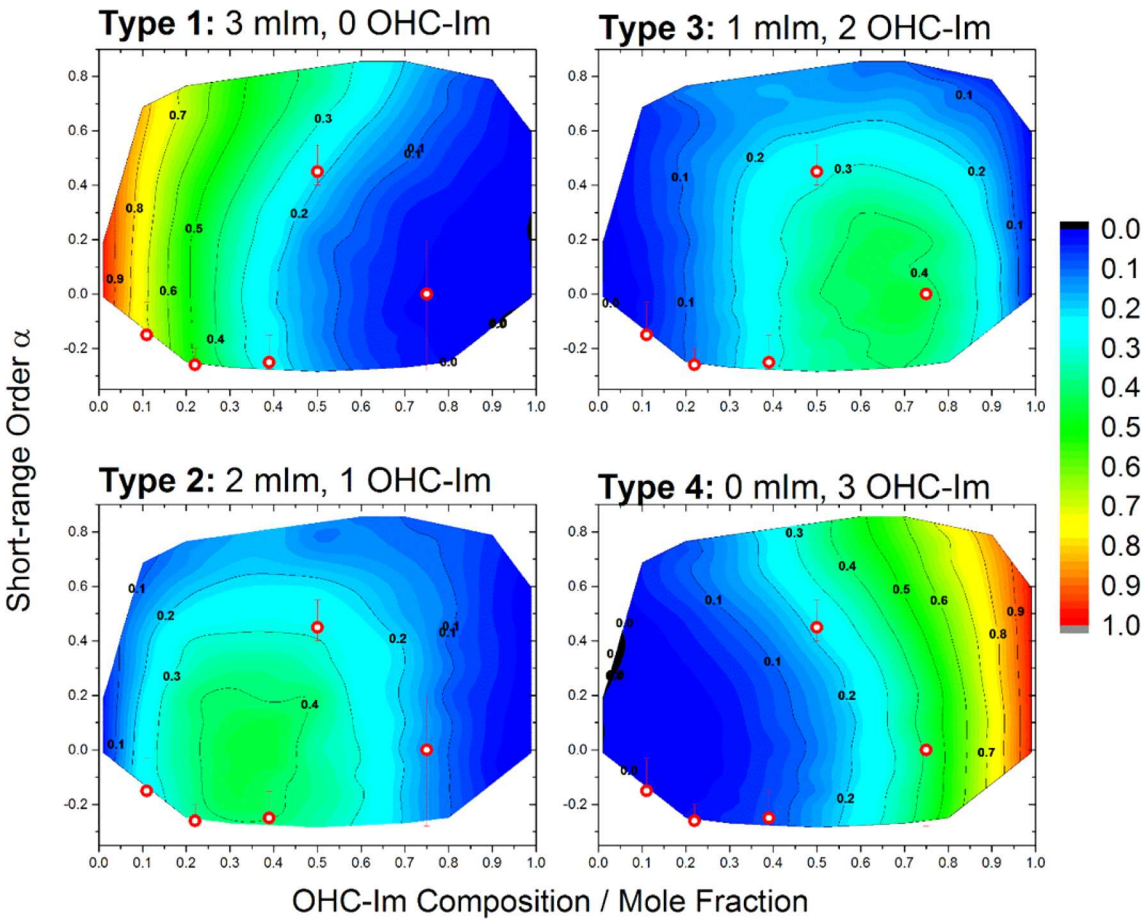

Figure 11. Probability distributions of observing the four possible types of pore windows as a function of the short-range order parameter (α) and the overall composition of the mixed-linker ZIF-8-90 material. Red circles indicate the window type probabilities for the experimental samples.

DOI: 10.1021/jacs.6b02754
J. Am. Chem. Soc. 2016, 138, 7325−7336

in a two-step method. A depth-first search (DFS) algorithm was applied that identified cycles of size N (i.e., all 6 member rings) in an undirected graph (i.e., SOD topology with Zn centers as nodes and linkers as edges). Once all the 6 member rings were identified and the mIm/OHC-Im linkers had been assigned according to the RMC procedure described above, an assignment algorithm identifies which three linkers (i.e., those with imidazole ring hydrogens in the plane of the window) belong to each 6 member ring window. The type of these three linkers determines the window type. No energetic parameters were taken into account for this analysis. Figure 11 shows four contour plots representing the fractional probabilities of observing each of the four window types for a structure with a given composition and short-range order. For example, structures with positive SROs (i.e., more clustered linkers) demonstrate lower probabilities of observing Type 2 and Type 3 windows. The locations of the five experimentally studied hybrid materials are shown by the red circles in each plot. The ZIF-8_{50}-90_{50} structure has very similar window probability profiles whether the linkers are clustered (+0.45) or alternating (−0.25). While outside the scope of the present study, the above method of differentiating the structural models based on window type distributions could be used to qualitatively predict the influence of SRO on diffusion properties.

CONCLUSIONS

We have determined the unit-cell-level mixing of linkers in mixed-linker ZIFs (specifically ZIF-8-90) using a combination of ^{1}H CRAMPS NMR spectroscopy and computational techniques. Direct experimental observations of linker mixing were accomplished by measuring the spin diffusion behavior between functional groups on the linkers. The experimental data were then compared to simulations based on a spin exchange model and proton positions from computationally generated mixed-linker ZIF structure models that use the short-range order (SRO) parameter as a measure of the ordering, clustering, or randomization of the linkers. The present method offers the advantages of not requiring isotope enrichment as well as a potentially reasonable way of predicting how subtle changes in structure can affect the pore/window-type distribution in mixed-linker materials. Our findings undeniably indicate that the linkers in ZIF-8-90 hybrids are mixed on the subunit cell length scale, and provide conclusive evidence that the synthesis of these mixed-linker ZIFs results in true hybrid materials as opposed to separated or clustered phases within the same crystal. When using the kinetic spin exchange model, we find that the mixed-linker ZIFs exhibit slightly different levels of linker mixing depending on the bulk composition. Furthermore, structures close to equimolar composition of the two linkers appear to have greater tendency for linker clustering than those with a majority content of one linker. Using the mixed-linker ZIF structures determined by the NMR experiments and modeling, we have also shown how the window-type distribution in experimentally synthesized mixed-linker ZIF-8-90 materials varies as a function of their composition. The above structural information can be further used for predicting, screening, or understanding the tunable adsorption and diffusion behavior of mixed-linker ZIFs. This technique can be potentially applied to any MOF system with linker functional groups containing protons that are distinguishable by NMR and topologies known a priori through crystallographic techniques.

ASSOCIATED CONTENT

Supporting Information

The Supporting Information is available free of charge on the ACS Publications website at DOI: 10.1021/jacs.6b02754.

Details of the synthesis of pure and mixed-linker ZIF materials, XRD patterns (experimental and simulated), representative SEM images, BET surface areas, and solution state NMR spectra, single pulse excitation spectra, calculation of second moment of NMR spectra, T2 curves, and detailed equations for semiempirical fitting of ^{1}H CRAMPS experimental data (PDF)

AUTHOR INFORMATION

Corresponding Author

*sankar.nair@chbe.gatech.edu

Author Contributions

‖These authors contributed equally.

Notes

The authors declare no competing financial interest.

ACKNOWLEDGMENTS

This work was supported by NSF-CBET #1264874. We are grateful to Prof. Sophia Hayes (Washington University in St. Louis) for detailed discussions on this work. Certain commercial equipment and materials are identified in this paper in order to specify adequately the experimental procedure. In no case does such identification imply recommendations by the National Institute of Standards and Technology, nor does it imply that the material or equipment identified is necessarily the best available for this purpose.

REFERENCES

(1) Park, K. S.; Ni, Z.; Cote, A. P.; Choi, J. Y.; Huang, R.; Uribe-Romo, F. J.; Chae, H. K.; O'Keeffe, M.; Yaghi, O. M. *Proc. Natl. Acad. Sci. U. S. A.* **2006**, *103*, 10186.

(2) Banerjee, R.; Phan, A.; Wang, B.; Knobler, C. B.; Furukawa, H.; O'Keeffe, M.; Yaghi, O. M. *Science* **2008**, *319*, 939.

(3) Phan, A.; Doonan, C. J.; Uribe-Romo, F. J.; Knobler, C. B.; O'Keeffe, M.; Yaghi, O. M. *Acc. Chem. Res.* **2010**, *43*, 58.

(4) Li, Y.; Liang, F.; Bux, H.; Yang, W.; Caro, J. *J. Membr. Sci.* **2010**, *354*, 48.

(5) Brown, A. J.; Johnson, J. R.; Lydon, M. E.; Koros, W. J.; Jones, C. W.; Nair, S. *Angew. Chem.* **2012**, *124*, 10767.

(6) Thornton, A. W.; Dubbeldam, D.; Liu, M. S.; Ladewig, B. P.; Hill, A. J.; Hill, M. R. *Energy Environ. Sci.* **2012**, *5*, 7637.

(7) Pimentel, B. R.; Parulkar, A.; Zhou, E.-k.; Brunelli, N. A.; Lively, R. P. *ChemSusChem* **2014**, *7*, 3202.

(8) Banerjee, R.; Furukawa, H.; Britt, D.; Knobler, C. B.; O'Keeffe, M.; Yaghi, O. M. *J. Am. Chem. Soc.* **2009**, *131*, 3875.

(9) Morris, W.; Leung, B.; Furukawa, H.; Yaghi, O. K.; He, N.; Hayashi, H.; Houndonougbo, Y.; Asta, M.; Laird, B. B.; Yaghi, O. M. *J. Am. Chem. Soc.* **2010**, *132*, 11006.

(10) Cousin Saint Remi, J.; Remy, T.; Van Hunskerken, V.; van de Perre, S.; Duerinck, T.; Maes, M.; De Vos, D.; Gobechiya, E.; Kirschhock, C. E. A.; Baron, G. V.; Denayer, J. F. M. *ChemSusChem* **2011**, *4*, 1074.

(11) Zhang, C.; Lively, R. P.; Zhang, K.; Johnson, J. R.; Karvan, O.; Koros, W. J. *J. Phys. Chem. Lett.* **2012**, *3*, 2130.

(12) Zhang, K.; Lively, R. P.; Zhang, C.; Koros, W. J.; Chance, R. R. *J. Phys. Chem. C* **2013**, *117*, 7214.

(13) Zhang, K.; Lively, R. P.; Dose, M. E.; Brown, A. J.; Zhang, C.; Chung, J.; Nair, S.; Koros, W. J.; Chance, R. R. *Chem. Commun.* **2013**, *49*, 3245.

DOI: 10.1021/jacs.6b02754
J. Am. Chem. Soc. 2016, 138, 7325−7336

(14) Zhang, K.; Lively, R. P.; Zhang, C.; Chance, R. R.; Koros, W. J.; Sholl, D. S.; Nair, S. *J. Phys. Chem. Lett.* **2013**, *4*, 3618.
(15) Thompson, J. A.; Blad, C. R.; Brunelli, N. A.; Lydon, M. E.; Lively, R. P.; Jones, C. W.; Nair, S. *Chem. Mater.* **2012**, *24*, 1930.
(16) Thompson, J. A.; Brunelli, N. A.; Lively, R. P.; Johnson, J. R.; Jones, C. W.; Nair, S. *J. Phys. Chem. C* **2013**, *117*, 8198.
(17) Eum, K.; Jayachandrababu, K. C.; Rashidi, F.; Zhang, K.; Leisen, J.; Graham, S.; Lively, R. P.; Chance, R. R.; Sholl, D. S.; Jones, C. W.; Nair, S. *J. Am. Chem. Soc.* **2015**, *137*, 4191.
(18) Rashidi, F.; Blad, C. R.; Jones, C. W.; Nair, S. *AIChE J.* **2016**, *62*, 525.
(19) Wu, Y.; Chen, H.; Liu, D.; Qian, Y.; Xi, H. *Chem. Eng. Sci.* **2015**, *124*, 144.
(20) Thornton, A. W.; Dubbeldam, D.; Liu, M. S.; Ladewig, B. P.; Hill, A. J.; Hill, M. R. *Energy Environ. Sci.* **2012**, *5*, 7637.
(21) Liu, B.; Smit, B. *J. Phys. Chem. C* **2010**, *114*, 8515.
(22) Liu, J.; Keskin, S.; Sholl, D. S.; Johnson, J. K. *J. Phys. Chem. C* **2011**, *115*, 12560.
(23) Haldoupis, E.; Watanabe, T.; Nair, S.; Sholl, D. S. *ChemPhysChem* **2012**, *13*, 3449.
(24) Clauss, J.; Schmidt-Rohr, K.; Spiess, H. W. *Acta Polym.* **1993**, *44*, 1.
(25) Mellinger, F.; Wilhelm, M.; Spiess, H. W. *Macromolecules* **1999**, *32*, 4686.
(26) Jia, X.; Wolak, J.; Wang, X.; White, J. L. *Macromolecules* **2003**, *36*, 712.
(27) Schmidt-Rohr, K.; Spiess, H. W. *Multidimensional solid-state NMR and polymers*; Academic Press, 1994.
(28) Rossini, A. J.; Zagdoun, A.; Lelli, M.; Canivet, J.; Aguado, S.; Ouari, O.; Tordo, P.; Rosay, M.; Maas, W. E.; Coperet, C.; Farrusseng, D.; Emsley, L.; Lesage, A. *Angew. Chem., Int. Ed.* **2012**, *51*, 123.
(29) Baias, M.; Lesage, A.; Aguado, S.; Canivet, J.; Moizan-Basle, V.; Audebrand, N.; Farrusseng, D.; Emsley, L. *Angew. Chem., Int. Ed.* **2015**, *54*, 5971.
(30) Kong, X.; Deng, H.; Yan, F.; Kim, J.; Swisher, J. A.; Smit, B.; Yaghi, O. M.; Reimer, J. A. *Science* **2013**, *341*, 882.
(31) Krajnc, A.; Kos, T.; Zabukovec Logar, N.; Mali, G. *Angew. Chem., Int. Ed.* **2015**, *54*, 10535.
(32) Kamakoti, P.; Sholl, D. S. *Phys. Rev. B: Condens. Matter Mater. Phys.* **2005**, *71*, 014301.
(33) Gee, J. A.; Chung, J.; Nair, S.; Sholl, D. S. *J. Phys. Chem. C* **2013**, *117*, 3169.
(34) Lee, M.; Goldburg, W. I. *Phys. Rev.* **1965**, *140*, A1261.
(35) Leskes, M.; Madhu, P. K.; Vega, S. *Chem. Phys. Lett.* **2007**, *447*, 370.
(36) Coelho, C.; Rocha, J.; Madhu, P. K.; Mafra, J. *J. Magn. Reson.* **2008**, *194*, 264.
(37) Nieuwendaal, R. C. *Solid State Nucl. Magn. Reson.* **2016**, *77*, 29.
(38) Morris, W.; Doonan, C. J.; Furukawa, H.; Banerjee, R.; Yaghi, O. M. *J. Am. Chem. Soc.* **2008**, *130*, 12626.
(39) Allen, F. *Acta Crystallogr., Sect. B: Struct. Sci.* **2002**, *58*, 380.
(40) Kresse, G.; Furthmüller, J. *Phys. Rev. B: Condens. Matter Mater. Phys.* **1996**, *54*, 11169.
(41) Sholl, D. S.; Steckel, J. A. *Density Functional Theory: A Practical Introduction*; John Wiley & Sons, Inc.: Hoboken, NJ, 2009.
(42) Perdew, J. P.; Burke, K.; Ernzerhof, M. *Phys. Rev. Lett.* **1996**, *77*, 3865.
(43) Grimme, S. *J. Comput. Chem.* **2006**, *27*, 1787.
(44) Newman, M. E. J.; Ziff, R. M. *Phys. Rev. E: Stat. Phys., Plasmas, Fluids, Relat. Interdiscip. Top.* **2001**, *64*, 016706.
(45) Macrae, C. F.; Bruno, I. J.; Chisholm, J. A.; Edgington, P. R.; McCabe, P.; Pidcock, E.; Rodriguez-Monge, L.; Taylor, R.; van de Streek, J.; Wood, P. A. *J. Appl. Crystallogr.* **2008**, *41*, 466.
(46) Macrae, C. F.; Edgington, P. R.; McCabe, P.; Pidcock, E.; Shields, G. P.; Taylor, R.; Towler, M.; van de Streek, J. *J. Appl. Crystallogr.* **2006**, *39*, 453.
(47) Bruno, I. J.; Cole, J. C.; Edgington, P. R.; Kessler, M.; Macrae, C. F.; McCabe, P.; Pearson, J.; Taylor, R. *Acta Crystallogr., Sect. B: Struct. Sci.* **2002**, *58*, 389.
(48) Taylor, R.; Macrae, C. F. *Acta Crystallogr., Sect. B: Struct. Sci.* **2001**, *57*, 815.
(49) Perrin, C. L.; Dwyer, T. J. *Chem. Rev.* **1990**, *90*, 935.
(50) Elena, B.; Emsley, L. *J. Am. Chem. Soc.* **2005**, *127*, 9140.
(51) Elena, B.; Pintacuda, G.; Mifsud, N.; Emsley, L. *J. Am. Chem. Soc.* **2006**, *128*, 9555.
(52) Suter, D.; Ernst, R. R. *Phys. Rev. B: Condens. Matter Mater. Phys.* **1985**, *32*, 5608.
(53) Henrichs, P. M.; Linder, M.; Hewitt, J. M. *J. Chem. Phys.* **1986**, *85*, 7077.
(54) Kubo, A.; McDowell, C. A. *J. Chem. Soc., Faraday Trans. 1* **1988**, *84*, 3713.
(55) VanderHart, D. L.; McFadden, G. B. *Solid State Nucl. Magn. Reson.* **1996**, *7*, 45.
(56) Spiegel, S.; Schmidt-Rohr, K.; Boeffel, C.; Spiess, H. W. *Polymer* **1993**, *34*, 4566.
(57) Willems, T. F.; Rycroft, C. H.; Kazi, M.; Meza, J. C.; Haranczyk, M. *Microporous Mesoporous Mater.* **2012**, *149*, 134.
(58) Chen, Q.; Schmidt-Rohr, K. *Solid State Nucl. Magn. Reson.* **2006**, *29*, 142.
(59) Kidron, A. *Phys. Lett. A* **1967**, *25A*, 112.

DOI: 10.1021/jacs.6b02754
J. Am. Chem. Soc. 2016, 138, 7325−7336